

Solving the relativistic inverse stellar problem through gravitational waves observation of binary neutron stars

Tiziano Abdelsalhin,^{1,*} Andrea Maselli,^{2,†} and Valeria Ferrari^{1,‡}

¹*Dipartimento di Fisica, Sapienza Università di Roma & Sezione INFN Roma1, P.A. Moro 5, 00185, Roma, Italy*

²*CENTRA, Departamento de Física, Instituto Superior Técnico - IST, Universidade de Lisboa, - UL, Avenida Rovisco Pais 1, 1049 Lisboa, Portugal*

(Dated: April 17, 2018)

The LIGO/Virgo collaboration has recently announced the direct detection of gravitational waves emitted in the coalescence of a neutron star binary. This discovery allows, for the first time, to set new constraints on the behavior of matter at supranuclear density, complementary with those coming from astrophysical observations in the electromagnetic band. In this paper we demonstrate the feasibility of using gravitational signals to solve the relativistic inverse stellar problem, i.e., to reconstruct the parameters of the equation of state (EoS) from measurements of the stellar mass and tidal Love number. We perform Bayesian inference of mock data, based on different models of the star internal composition, modeled through piecewise polytropes. Our analysis shows that the detection of a small number of sources by a network of advanced interferometers would allow to put accurate bounds on the EoS parameters, and to perform a model selection among the realistic equations of state proposed in the literature.

I. INTRODUCTION

Decades of experimental and theoretical efforts have finally led gravitational wave astronomy to emerge as a new field of research and an extraordinary lookout on the high energetic phenomena of our Universe. After the first binary black hole coalescence observed by LIGO [1–3], Advanced Virgo has recently joined the quest, leading to the discovery of a further double black hole system, greatly improving the capability to localize the source [4]. More recently, the LIGO/Virgo collaboration has announced the first detection of a gravitational wave (GW) signal associated to the inspiral of two coalescing neutron stars [5]. GW170817 also is the first astrophysical event observed simultaneously in both the gravitational and electromagnetic bands: a short gamma ray burst detected in coincidence has marked the dawn of the multimessenger astronomy [6].

At design sensitivity, LIGO and Virgo are expected to detect almost one binary neutron star (NS) per week. This incoming flood of data will be extremely precious to test gravity in a strong field regime, and to investigate the behavior of matter in extreme conditions. Neutron star cores are characterized by densities which may exceed the nuclear saturation point $\rho_0 \sim 2.7 \times 10^{14} \text{ g/cm}^3$. A rigorous and comprehensive description of matter in this regime is currently unavailable. The lack of experimental data and the complexity of modeling two and three-body strong interactions at $\rho \gg \rho_0$ leads to large uncertainties on the star equation of state. Various theoretical approaches have been developed so far, that predict different scenarios for the nuclear matter, including

mixture of $npe\mu$ in β -equilibrium, hyperon production, meson condensates and phase transitions to deconfined quarks [7].

It is known that the equation of state of matter $p = p(\epsilon)$, which links pressure and energy density, can be mapped to a mass-radius relation using the equation of stellar structure [8]; these link the microscopic properties of matter to the macroscopic properties of the star, the radius R and the mass M . A complete knowledge of the $M(R)$ profile could, in principle, be inverted in order to determine the EoS. However, observational uncertainties, and a limited number of simultaneous measurements of NS observables, are the largest obstacles in solving the *relativistic inverse stellar problem* to constrain the nuclear equation of state [8].

In the last years, gravitational waves from binary NSs or NS-black hole mergers have been invoked as precious source of information, possibly able to shed new light on the star internal composition [9–15]. In this regard, the recent detection of the GW170817 event provides a striking confirmation of the new prospects offered by GW astronomy [5]. The imprint of the equation of state on the gravitational signal shows up during the last phases of the inspiral¹, when tidal interactions play a significant role and are strong enough to induce a quadrupolar deformation in the NSs, that affects the phase of the emitted waveform. In the adiabatic approximation, the induced quadrupole moment Q_{ij} is proportional to the external tidal field \mathcal{E}_{ij} , $Q_{ij} = -\lambda \mathcal{E}_{ij}$, where λ is the NS *tidal deformability*, which encodes the deformation properties of the star [18–20]. For a given compactness M/R , λ depends on the equation of state only. Therefore, binary

* tiziano.abdelsalhin@roma1.infn.it

† andrea.maselli@tecnico.ulisboa.pt

‡ valeria.ferrari@roma1.infn.it

¹ A footprint of the star EoS is also present in the postmerger signal (see for example [16, 17] and references therein). The analysis of this part of the waveform is however outside the scope of this paper.

mergers containing at least one NS offer a new possibility to constrain the EoS of matter at supranuclear densities. GW170817 has already set interesting constraints on the tidal deformability [5], which favour low stellar compactness and hence soft matter, in agreement with astrophysical measurements in the electromagnetic bandwidth [21].

In principle, multiple observations of isolated and binary NSs may provide a collection of pairs $[M, R]$ or $[M, \lambda]$, dense *and* accurate enough to map the correct EoS. However, error bars on these quantities are still large, especially on R and λ , and the proposed EoSs depend on several parameters arising on the way hadron interactions are modeled and on the particle content. Phenomenological parametrizations of the NS equation of state provide an effective approach to solve the inverse stellar problem [22], since they allow to describe a large class of EoSs through a relatively small set of coefficients, to be constrained by astrophysical data. These EoSs can then be used to combine measurements of different NS parameters, exploiting the results of gravitational and electromagnetic surveys to obtain genuine multi-wavelength constraints on the EoS [23]. Moreover, it may be possible that the *true* equation of state differs from the models proposed in literature so far. In this case, a phenomenological approach would be extremely useful to constrain the main features of the correct EoS.

Phenomenological models developed so far include: (i) a spectral representation in terms of the enthalpy, proposed by Lindblom and collaborators [24, 25], (ii) the piecewise polytropic equation of state developed by Read et al. in [26], (iii) the model described by Steiner [27], in which the EoS is divided into four density regimes: a fixed crust below the nuclear saturation point ρ_0 , one pressure-energy relation depending on nuclear physics parameters (as symmetry energy and proton/electron fraction) for $\rho \simeq \rho_0$, and two polytropic relations at larger densities to fit the inner core.

In this paper we show how GW signals emitted by coalescing binary neutron stars can be used to solve the relativistic inverse stellar problem, and to infer the EoS parameters of the piecewise polytropic parametrization. We generate data of masses and tidal deformabilities for two classes of EoSs which span a large range of compactness, determining the minimum number of observations needed to fully constrain the EoS. We perform a Bayesian analysis by considering a network of advanced interferometers, composed by LIGO, Virgo and the upcoming KAGRA. Our results suggest that few GW detections may already be able to set accurate constraints on some of the piecewise parameters, that can be used to make model selection among various realistic EoS.

The plan of the paper is the following: In Sec. II we describe the main properties of the phenomenological parametrization used to model the NS equation of state, and the classes of EoS considered in this paper. In Secs. III-IV we outline the numerical approach developed to constrain the parameters of the EoS from GW observation. The results of our analysis are presented in

Sec. V, where we also show how the reconstructed parameters can be used to discriminate among different EoSs. Concluding remarks are summarized in Sec. VI.

Throughout the paper we use geometrized units, in which $G = c = 1$.

II. THE EQUATION OF STATE

As already mentioned in the introduction, a complete and detailed description of NS matter at supranuclear densities is still missing. This uncertainty yields different mass-radius relations, corresponding to distinct *realistic* EoS, to be constrained by observational data. These will ultimately allow to characterize the behavior of nuclear forces at $\rho \gg \rho_0$ and to identify the correct approach. However, the complexity of such models has motivated the quest for phenomenological frameworks, which capture the main features of the behavior of nuclear matter and can reproduce tabulated EoS. Among the various models proposed so far, we focus on piecewise polytropic equations of state in its original formulation [26], although some variations² have been also considered in literature [30].

Piecewise polytropes accurately fit the energy-density profiles of a large variety of EoSs based on realistic nuclear-physics calculations. These include pure nucleonic matter, hyperons, meson condensates and phase transitions to deconfined quarks. The NS macroscopic observables, like masses and radii, are accurately reproduced within $\lesssim 1\%$ of the corresponding “exact” values. This accuracy is achieved requiring that the high-density core is represented by three polytropic segments

$$p(\rho) = K_i \rho^{\Gamma_i} \quad \rho_{i-1} \leq \rho \leq \rho_i, \quad (1)$$

specified by the dividing rest-mass densities, with adiabatic constant and index given by K_i and Γ_i , respectively. Read and collaborators found that the values of the dividing densities which minimize the discrepancy with respect to the tabulated EoSs correspond to $\rho_1 = 10^{14.7} \text{ g/cm}^3$ and $\rho_2 = 10^{15} \text{ g/cm}^3$. A schematic picture of this model is shown in Fig. 1.

The energy density ϵ is given by the integral of the first law of thermodynamics:

$$d\epsilon = \frac{(\epsilon + p)}{\rho} d\rho, \quad (2)$$

which can be recast through Eq. (1) to the following form

$$\epsilon(\rho) = (1 + a_i)\rho + \frac{p(\rho)}{\Gamma_i - 1}, \quad (3)$$

² In this regard, Raithel *et al.* have recently shown that NS masses and radii measured by electromagnetic surveys may be exploited to reconstruct some features of the parametrized EoS [28, 29].

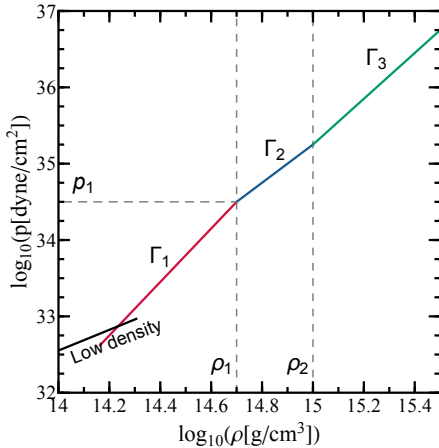


FIG. 1. Schematic representation of the dividing regions which specify the piecewise representation of the NS structure. The inner and center pieces are separated by the dividing densities $\rho_{1,2}$, fixed to $\rho_1 = 10^{14.7} \text{ g/cm}^3$ and $\rho_2 = 10^{15} \text{ g/cm}^3$, respectively. Adapted from [26].

where a_i are integration constants to be determined requiring continuity between the three regions. Specifying the initial density of the outer interface reduces the number of independent parameters to four variables, namely $\{p_1, \Gamma_1, \Gamma_2, \Gamma_3\}$, where $p_1 \equiv \log_{10} p(\rho_1)$. As we will discuss in the next section, the latter is the actual quantity to be constrained through the inverse stellar approach.

At low densities, the last interface is matched dynamically to a fixed crust, which is chosen to be a parametrized four-piece polytropic version of the SLy EoS. The matching point is simply given by the value of density where the crust and core-EoS intersect each other, and depends only on p_1 and Γ_1 . This choice naturally implies a constraint on these two parameters, since specific combinations of p_1 and Γ_1 do exist, which yield no intersection between the crust and the core EoSs and are therefore incompatible. The allowed region can be found analytically, and satisfies the following relation

$$\Gamma_1 > \frac{\log\left(\frac{p(\rho_1)}{p_{\text{sly}}}\right)}{\log\left(\frac{\rho_1}{\rho_{\text{sly}}}\right)}, \quad (4)$$

where ρ_{sly} and p_{sly} are the density and the pressure in the inner region of the crust.

Figure 2 shows the mass-radius relations obtained by solving the relativistic equations of stellar structure for different EoSs, modeled through the piecewise parametrization. Details on the various EoS can be found in Section II of [26].

III. THE MARKOV CHAIN MONTE CARLO

In this section we shall describe the numerical approach we use to estimate the piecewise parameters,

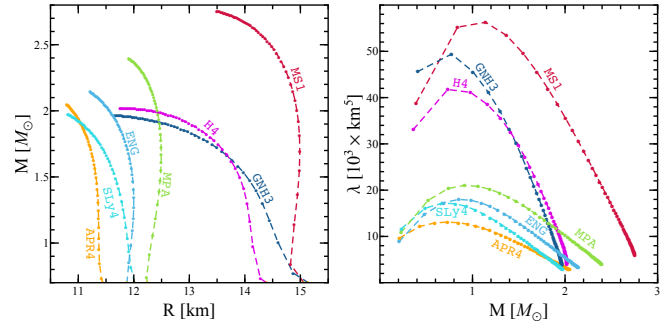


FIG. 2. (Left) Mass-radius relations for some realistic EoSs modeled through piecewise polytropes. The values of the parameters $\{p_1, \Gamma_1, \Gamma_2, \Gamma_3\}$ which specify the EoS can be found in Table III of [26]. (Right) Tidal deformability λ as a function of the NS mass for the same EoS considered in the left panel.

starting from the macroscopic observables provided by gravitational wave observations, namely the mass M and the tidal deformability λ of detected NSs. It is worth noting that our method is completely general, and can be applied also using different NS observables, obtained either with electromagnetic or gravitational wave observations, leading to a genuine multimessenger framework [23].

In general, for a given set of N observed stars, we have $m+N$ free parameters to determine, i.e., m parameters of the EoS model, and N central pressures $p_{i=1\dots N}^c$. Any detected NS provides 2 observables, which we have assumed to be the mass and the tidal deformability. Therefore, to fully characterize the parametrized EoS, we need at least $N = m$ observations.

As discussed in Sec. II, piecewise polytropes are characterized by $m = 4$ parameters, which lead to 8 unknown parameters to be found:

$$\vec{\theta} = \{p_1, \Gamma_1, \Gamma_2, \Gamma_3, p_1^c, p_2^c, p_3^c, p_4^c\};$$

therefore, we need at least 4 observations, which provide the required set of 8 measured quantities $\vec{d} = \{M_i, \lambda_i\}_{i=1\dots 4}$.

Within Bayesian inference, we are interested in determining the posterior probability density function (PDF) of the EoS parameters given the experimental data: $\mathcal{P}(\vec{\theta}|\vec{d})$. Using Bayes' theorem, we can write the joint PDF for EoS parameters as:

$$\mathcal{P}(\vec{\theta}|\vec{d}) \propto \mathcal{P}_0(\vec{\theta}) \mathcal{L}(\vec{d}|\vec{\theta}), \quad (5)$$

where $\mathcal{P}_0(\vec{\theta})$ describes the prior information on the parameters, and $\mathcal{L}(\vec{d}|\vec{\theta})$ is the likelihood function. The probability distribution of l parameters is given by marginalizing over the remaining $N+4-l$ variables, i.e.,

$$\mathcal{P}(\theta_1, \dots, \theta_l) = \int \mathcal{P}(\vec{\theta}) d\theta_{l+1} \dots d\theta_{N+4}. \quad (6)$$

In our analysis we assume that the set of data \vec{d} obtained from GW detections are independent and Gaussian distributed, with the values of each observable M_i (λ_i) being affected by an experimental uncertainty σ_{M_i} (σ_{λ_i}). Under this assumptions the likelihood can be written as $\mathcal{L} \propto e^{-\chi^2}$, where the chi-square variable reads:

$$\chi^2 = \frac{1}{2} \sum_{i=1}^N \left\{ \frac{[M(p_1, \Gamma_1, \Gamma_2, \Gamma_3, p_i^c) - M_i]^2}{\sigma_{M_i}^2} + \frac{[\lambda(p_1, \Gamma_1, \Gamma_2, \Gamma_3, p_i^c) - \lambda_i]^2}{\sigma_{\lambda_i}^2} \right\}. \quad (7)$$

We sample the posterior probability distribution (5) using Markov chain Monte Carlo (MCMC) simulations based on the Metropolis-Hastings algorithm [31]. The procedure of this framework can be summarized with the following steps.

Given an initial point $\vec{\theta}_1 = \{p_1, \Gamma_1, \Gamma_2, \Gamma_3, p_{i=1 \dots N}^c\}$, randomly chosen within the parameter space, we propose a jump to a new state, $\vec{\theta}_2$, with probability specified by the proposal function $f = f(\vec{\theta}_1, \vec{\theta}_2)$. The latter is chosen to be a multivariate Gaussian distribution³ centered in the current state $\vec{\theta}_1$, $f(\vec{\theta}_2, \vec{\theta}_1) = \mathcal{N}(\vec{\theta}_1, \Sigma)$. Then, we compute the ratio

$$r(\vec{\theta}_1, \vec{\theta}_2) = \frac{\mathcal{P}(\vec{\theta}_2)}{\mathcal{P}(\vec{\theta}_1)}, \quad (8)$$

and accept the proposed move with probability

$$a(\vec{\theta}_1, \vec{\theta}_2) = \min \left\{ 1, r(\vec{\theta}_1, \vec{\theta}_2) \right\}. \quad (9)$$

In this way, the chain is updated to the step $\vec{\theta}_2$ with probability $a(\vec{\theta}_1, \vec{\theta}_2)$, or remains fixed in $\vec{\theta}_1$ with probability $1 - a(\vec{\theta}_1, \vec{\theta}_2)$. If $\mathcal{P}(\vec{\theta}_2) \geq \mathcal{P}(\vec{\theta}_1)$ the jump is always accepted, while if $\mathcal{P}(\vec{\theta}_2) < \mathcal{P}(\vec{\theta}_1)$ it is accepted with probability $r(\vec{\theta}_1, \vec{\theta}_2)$. The previous steps are then iterated n times, allowing the chain to explore the parameter space of the model (a workflow is shown in Algorithm 1). MCMC theory guarantees that, from any initial state and proposal function, the system evolves towards the desired target distribution $\mathcal{P}(\vec{\theta})$. In practical situations however, the convergence of the chain is strongly affected by the choice of the proposal function. In this paper we adopt an adaptive framework, in which the covariance Σ of $f(\vec{\theta}_1, \vec{\theta}_2)$ is continuously updated through a *Gaussian adaptation* algorithm (GaA) [32]. A remarkable feature of this approach is that the acceptance probability P of the proposed jump can be fixed a priori (a detailed description of the formalism is presented in Appendix VI).

³ Note that with this choice f is symmetric, i.e., $f(\vec{\theta}_2, \vec{\theta}_1) = f(\vec{\theta}_1, \vec{\theta}_2)$.

IV. NUMERICAL SETUP

In order to test the ability of our approach to reconstruct the parameters of the piecewise polytropes, we have analyzed different possible scenarios. We consider nonspinning NSs with $M \in [1.1 - 1.6]M_\odot$, which covers most of the mass range determined so far by electromagnetic observations of binary pulsars [21]. Moreover, we focus on two EoS, **apr4** and **h4**. As shown in Fig. 2, these models span a wide range of mass-radius configurations. Moreover they fit within the 90% credible interval estimated by the LIGO/Virgo collaboration after the first GW detection from a binary NS [5, 33]. Therefore, **apr4** and **h4** are the best candidates to represent extreme cases of *soft* and *stiff* nuclear matter, compatible with astrophysical observations. For both EoSs, we compare the features of a canonical $1.4M_\odot$ NS in Table I, which also shows how the tidal deformability of the two EoS differs by a factor > 3 . We remember that large values of λ yield stronger changes in the GW signal, and therefore lead to tighter constraints.

TABLE I. Radius and tidal deformability of prototype $1.4M_\odot$ NSs modeled with **apr4** and **h4**.

EoS	R_{NS} [km]	λ [km ⁵]
apr4	11.34	9502
h4	13.99	32861

It is important to stress that for $M \lesssim 1.6M_\odot$ the adiabatic index Γ_3 does not affect the structure of the star for both **apr4** and **h4**. Therefore, we can safely neglect this coefficient within the analysis, reducing the parameter space volume to $\vec{\theta} = \{p_1, \Gamma_1, \Gamma_2, p_1^c, p_2^c, p_3^c\}$. Note that the EoS is now fully specified by only three variables, and as a consequence we only need six observables, which correspond to three observed NSs. No observational constraints have been derived so far for the Love numbers of a neutron star⁴. Therefore, we compute σ_λ using a Fisher matrix approach [34], and considering equal-mass binary NSs at prototype distance of 100 Mpc.

The uncertainties are computed for the advanced generation of detectors. More specifically, we will assume that the GW events have been detected by a network⁵ of interferometers (HLVK) composed by the two LIGO sites, Virgo and the Japanese KAGRA. For all the measurements we consider detector's configurations at design

⁴ The gravitational wave event GW170817 has actually allowed to set an upper bound on the *average* tidal deformability of the two stars, $\tilde{\Lambda} \leq 800$, where

$$\tilde{\Lambda} = \frac{16}{13m^5} \left[\frac{m_1 + 12m_2}{m_1} \lambda_1 + \frac{m_2 + 12m_1}{m_2} \lambda_2 \right],$$

being $(m_1 + m_2)$ the total mass of the binary [5].

⁵ Note that for a N independent interferometers the error on the Love number is roughly reduced by a factor $\sim 1/\sqrt{N}$, with respect to the single detector analysis.

sensitivity [35–37]. Moreover, following [38], we fix the uncertainty on the NS mass, σ_M to 10% of the measured value for HLVK. We choose flat prior distributions for all the parameters of the piecewise EoS, within the range $p_1 \in [33, 35]$, $\Gamma_{1,2} \in [1, 4]$ and $p_i^c \in [10^{-6}, 10^{-3}] \text{ km}^{-2}$. The adiabatic index and the initial pressure of the outer core, (Γ_1, p_1) , are also constrained by the theoretical bound given by Eq. (4). Finally, for each set of data, we run four parallel processes of $n = 5 \times 10^5$ samples. We assess the convergence of the MCMC simulations to the target distribution through the Rubin test, and by analyzing the autocorrelation of each chain [31].

V. RECONSTRUCT THE EOS PARAMETERS

The first goal of our approach is to determine the parameters of the piecewise EoS. As described in Sec. IV we have 6 unknown variables to constrain, i.e., $\vec{\theta} = \{p_1, \Gamma_1, \Gamma_2, p_1^c, p_2^c, p_3^c\}$, which require three NS observations. For the sake of clarity, we will test our method on the following prototype configurations: (i) the model **m246** with three objects of mass $(1.2, 1.4, 1.6)M_\odot$, (ii) a *heavier* one **m456** composed of stars of $(1.4, 1.5, 1.6)M_\odot$, (iii) a *lighter* system **m123** with masses $(1.1, 1.2, 1.3)M_\odot$.

Figure 3 shows the marginalized posterior distributions of the piecewise parameters corresponding to the **apr4** EoS, derived for **m246**. The dashed vertical line in each panel indicates the true value of the parameter, while the darker bands correspond to the 1σ credible intervals. The numerical values of injected and reconstructed parameters are also listed in Table II for the considered configurations and for the EoS **apr4** and **h4**.

At a first glance, we immediately note that the true values of all the parameters are always reconstructed within the 1σ confidence level. The posteriors of the NSs' central pressures are always peaked around the injected values with nearly symmetrical distributions. The dividing pressure p_1 is also extremely well measured, with the relative difference between the expected valued and the median being below 1%.

In general, the adiabatic indices of the piecewise representation are determined with less accuracy, although some differences do exist between the various polytropic segments. The top panels of Fig. 3 show indeed that Γ_1 is unconstrained, with an almost flat posterior within the allowed range of values. Conversely, the second index Γ_2 provides better results, with a median close to the true quantity, and a probability distribution that tends to favor larger values. Analyzing the joint distribution between various parameters we find that p_1 - Γ_2 is the only pair that shows a significant correlation, which is, otherwise, very small. As we shall see in the next section, this feature is crucial in order to exploit the piecewise representation to distinguish different EoS.

Most of the features described so far do not change qualitatively if we analyze the other two models **m456** and **m123**, for the same EoS **apr4**. Smaller masses lead

in general to stronger constraints. This is somehow expected since, for a fixed EoS, lighter NSs yield larger Love numbers which enhance the tidal contribution to the GW signal and therefore provide smaller errors σ_λ .

A direct comparison between the posterior distribution of p_1 and Γ_2 obtained for the three configurations we consider, is shown in Fig. 4. In both panels the best results occur for the model **m123**, which is composed of three NSs with masses $(1.1, 1.2, 1.3)M_\odot$, and the shape of the distribution is similar to that of **m246**. Conversely, for **m456** which considers a collection of data with heavier objects, the posterior distributions of both p_1 and Γ_2 broaden significantly and the 1σ level becomes much looser.

The picture described above changes qualitatively when we consider NSs made of a stiffer EoS, which leads to more deformable objects. As an example, in Fig. 5 we show the probability distributions of the piecewise parameters for the model **m246**, assuming **h4** as the underlying equation of state. We do not plot the central pressures p_i^c as they are not of great interest in our analysis, although they are found with an accuracy comparable with that shown in Fig. 3. The left panel of the figure shows that the dividing pressure p_1 is, again, the parameter which is constrained with the largest precision, the posterior distribution being nearly Gaussian and symmetric around the true value. However, a direct comparison with Fig. 3 shows that the role of the adiabatic indices Γ_1 and Γ_2 seems now to be reverted. Indeed, for the EoS **h4** it is Γ_1 which is very well estimated, with a relative difference of the median with respect to the true value smaller than 1%. The parameter Γ_2 is essentially unbounded, with a posterior distribution which is nearly flat.

The different features of the results for the two EoSs can be understood by looking at Fig. 6, where we plot, for each NS and EoS considered for **m246**, the radial distance $R(\rho)$ normalized to the radius of the star, as a function of the density ρ . The major difference between the two EoSs is that the radial profiles of the **apr4** stars extend to larger values of ρ , well inside the region of the second branch of the piecewise polytropic specified by Γ_2 ; conversely, the **h4** stars are mainly dominated by the first branch specified by Γ_1 . For this EoS, NSs with masses below $1.2M_\odot$ have a central pressure smaller than p_1 , and therefore are outside the Γ_2 interval (see Fig. 1).

Figure 6 also shows that at the boundary between the first two regions, the function $R(\rho)$ of the **apr4** stars is already between 80% and 90% of its overall value. Therefore, it seems quite natural that for this EoS the Love number, which is proportional to R_{NS}^5 , is more sensible to variations of Γ_2 . Conversely, the radius of the **h4** stars is almost completely determined by the integration of the stellar equations within the density region belonging to the first polytropic branch, and this is why the inverse stellar problem constrains Γ_1 with a larger accuracy.

This picture is strongly enhanced for low mass NSs, as can be noticed comparing the right panel of Fig. 5 and

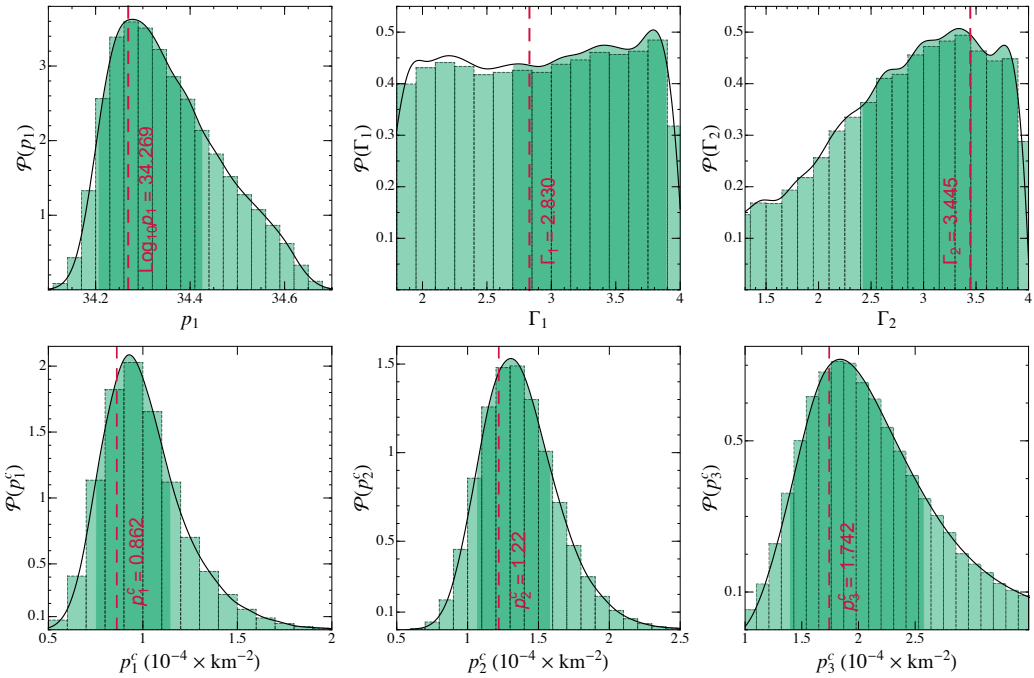


FIG. 3. Marginalized probability distributions for the piecewise parameters of the **apr4** EoS, derived for the **m246** model with NS masses $(1.2, 1.4, 1.6)M_{\odot}$, obtained for the network HLVK. The histograms of the sampled points are showed below each function. Dashed vertical lines identify the injected true values, while the shaded bands correspond to the 1σ credible regions of each parameter.

TABLE II. Comparison between injected and reconstructed values of the **apr4** and **h4** parameters for the three models analyzed in this paper. For each parameter of the piecewise EoS we show the 1σ credible level of the marginalized distribution.

EoS	m246			m456			m123		
	injected	1σ	injected	1σ	injected	1σ	injected	1σ	injected
apr4	p_1	34.269	[34.205 - 34.427]	34.269	[34.247 - 34.582]	34.269	[34.209 - 34.367]		
	Γ_1	2.830	[2.700 - 3.896]	2.830	[2.212 - 3.846]	2.830	[2.458 - 3.898]		
	Γ_2	3.445	[2.415 - 3.907]	3.445	[1.817 - 3.599]	3.445	[2.691 - 3.952]		
	$10^{-4} \times p_1^c$	0.862	[0.750 - 1.15]	1.22	[1.09 - 1.76]	0.722	[0.623 - 0.919]		
	$10^{-4} \times p_2^c$	1.22	[1.06 - 1.58]	1.45	[1.29 - 2.12]	0.862	[0.752 - 1.07]		
	$10^{-4} \times p_3^c$	1.74	[1.39 - 2.58]	1.74	[1.46 - 2.70]	1.03	[0.893 - 1.26]		
h4	p_1	34.669	[34.611 - 34.738]	34.669	[34.628 - 34.742]	34.669	[34.644 - 34.771]		
	Γ_1	2.909	[2.479 - 3.401]	2.909	[1.956 - 3.906]	2.909	[2.752 - 3.520]		
	Γ_2	2.246	[1.732 - 3.518]	2.246	[1.056 - 2.383]	2.246	[1.055 - 3.596]		
	$10^{-4} \times p_1^c$	0.372	[0.310 - 0.446]	0.533	[0.423 - 0.643]	0.311	[0.260 - 0.355]		
	$10^{-4} \times p_2^c$	0.533	[0.486 - 0.614]	0.650	[0.556 - 0.773]	0.372	[0.330 - 0.427]		
	$10^{-4} \times p_3^c$	0.804	[0.721 - 0.930]	0.804	[0.706 - 0.957]	0.443	[0.407 - 0.512]		

the left panel of Fig. 4, where we plot $\mathcal{P}(p_1)$ for the EoS **h4** and **apr4**, respectively. For the lightest configuration **m123**, the MCMC is able to accurately recover the value of p_1 for **apr4**. On the other hand, the reconstructed value for **h4** shows an offset with respect to the injected parameter.

This result can be traced back again to Fig. 6, which shows that for a $1.2M_{\odot}$ star, the radius depends only weakly on the adiabatic index Γ_1 , and it is dominated by the contributions coming from the low density part of the EoS. In particular, sampling the parameter space, we have found that the subspace $p_1-\Gamma_1$ is characterized

by a large region in which the posterior distribution assumes values only slightly lower than the absolute maximum, making extremely difficult to resolve it through the Monte Carlo simulation. As a consequence, the marginalized distributions are shifted with respect to the injected values.

The relativistic inverse stellar problem provides a powerful framework to perform EoS selection, i.e., to rule out models which are incompatible with astrophysical observations. Most notably, it provides a straightforward method to combine measurements with different NS masses and avoiding the quest for approximations which

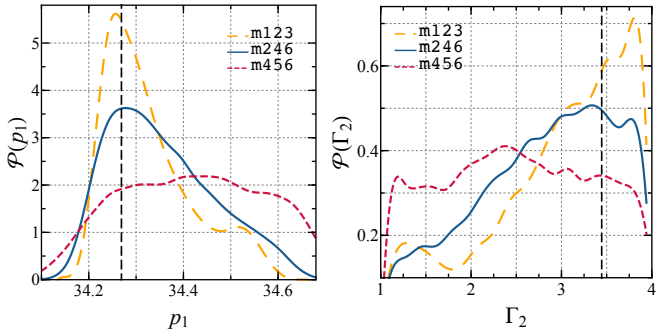


FIG. 4. Comparison among the marginalized posterior of p_1 (left) and Γ_2 (right) for **apr4**, derived for the models **m246**, **m456** and **m123**. The dot-dashed vertical lines correspond to the true values of the parameters.

relates λ and M [39]. Our study shows that for soft (stiff) matter, the joint probability distribution of p_1 - Γ_2 (p_1 - Γ_1) offers the best prospects for EoS selection. To better clarify this statement, in the left panels of Figs. 7–8 we show, for the configuration **m246**, the 1- and 2σ credible regions obtained from the posterior distributions of the parameters p_1 - Γ_2 for **apr4**, and p_1 - Γ_1 for **h4**, respectively. The red cross indicates the injected value, whereas the different markers are the values of the parameters corresponding to various equations of state which have been mapped on the piecewise polytropic in [26].

For both EoSs, the joint distributions seems quite effective in selecting the correct EoS. If the true EoS of supranuclear matter is stiff, measuring the Love numbers with sufficient accuracy would allow us to essentially rule out almost all known EoSs at more than 3σ level. If the true EoS is soft, being more similar to **apr4**, our ability would worsens, although we may still be able to constrain a portion of the parameter space. The right panels of Figs. 7–8 show how these bounds slightly change for the various mass configurations which we have analyzed.

VI. CONCLUSIONS

The detection of GW170817 opens the possibility to study the behavior of matter at supranuclear densities using gravitational waves as a probe. Indeed, even with a single event the LIGO-Virgo collaboration has set a constraint on the average tidal deformability $\tilde{\Lambda}$, an EoS-dependent parameters which appears in the GW signal, that favours high compact stars. In the next future, the detection of more events, possibly with larger signal-to-noise ratio, will sensibly strengthen our capability to constrain the NS equation of state with increasing accuracy.

In this work we have presented a Bayesian approach to reconstruct the parameters which characterize the EoS in the neutron star core, using masses and tidal Love numbers obtained from GW detections. We have developed our analysis modeling the EoS with a piecewise poly-

tropic, and generating the mock data using a *soft* and a *stiff* EoS which, compatibly with the constraint already put by GW170817, encompasses the range of admissible equations of state of nuclear matter.

Our results show that three observations of coalescing neutron star binaries, by a network of four advanced interferometers—two for LIGO, plus Virgo and KAGRA—would be sufficient to set interesting constraints on the parameters of the piecewise polytropic.

The true values of the parameters are always reconstructed within 1σ credible intervals. The parameter which is determined with the largest accuracy is the pressure p_1 , which identifies the interface between the first and second polytropic branch (see Fig. 1). In the most favorable scenario, the error can be smaller than 1%.

On the other hand, bounds on the polytropic indices are strongly affected by the stiffness of the EoS of the mock data. If the EoS is soft (stiff) the smaller error is obtained for the parameter which characterizes the inner (outer) part of the core. We also find that the central pressures of the NSs are always determined with an accuracy of the order of 10%.

Constraints on different parameters can be used to make EoS selection. In particular, we have found that the joint-2D posterior distribution for $p_1 - \Gamma_2$ (for soft matter) or $p_1 - \Gamma_1$ (for stiff matter) is the best tool to rule out EoS not in agreement with GW observations.

The method presented in this paper can easily be generalized in several directions by: (i) including a larger set of masses and tidal Love numbers obtained from multiple GW events, (ii) combining different NS observables obtained from astrophysical observations in the electromagnetic waveband and GW data, (iii) comparing the various phenomenological EoS available in literature in order to find the model which leads to the most accurate constraints. The second point is of particular interest, since parametrized EoSs are the straightforward approach to develop multimessenger strategies. A detailed analysis of how spectroscopic observations of NS radii may be combined with GW data is already under investigation, and will be presented in a forthcoming publication [23].

ACKNOWLEDGEMENTS

T.A. was partially supported by the “NewCompStar,” COST Action MP1304. T.A. also thanks Kostas Kokkotas for the kind hospitality during his stay at the University of Tübingen. A.M. acknowledges financial support provided under the European Union’s H2020 ERC Consolidator Grant “Matter and strong-field gravity: New frontiers in Einstein’s theory” grant agreement no. MaGRaTh-646597.

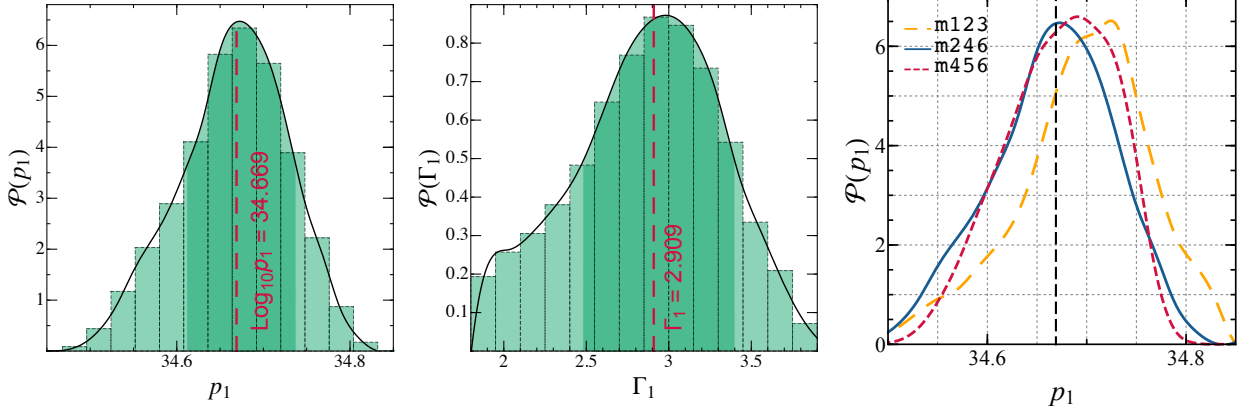


FIG. 5. (Left and center) Same as Fig. 3 but for the h4 EoS. (Right) We compare the posterior probability of p_1 for the models m246, m456, m123 and the EoS h4. The vertical dashed line marks the injected value.

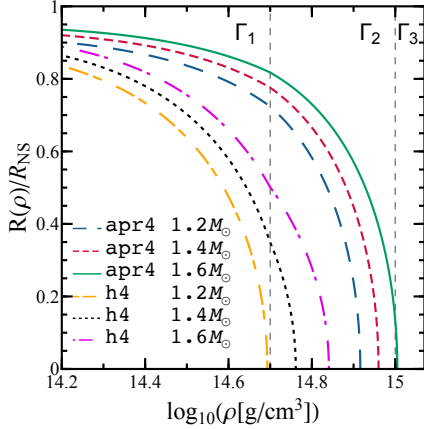


FIG. 6. The radial distance from the center of the star, normalized to its radius, is plotted as a function of density. Different curves and colors correspond to the masses and EoSs analyzed in the paper. The vertical lines separate the three regions of the piecewise parametrization.

APPENDIX: THE PROPOSAL MATRIX

According to the algorithm GaA, the covariance matrix Σ of the proposal distribution $f(\vec{\theta}_1, \vec{\theta}_2)$ is defined as

$$\Sigma = (\rho \mathbf{Q}) (\rho \mathbf{Q}^T) \quad (10)$$

where ρ is the step size of the algorithm and \mathbf{Q} the square root of the covariance matrix, normalized such that $\det(\mathbf{Q}) = 1$ [32, 40]. We compute \mathbf{Q} from Σ using the Cholesky decomposition.

Algorithm 1 Adaptive Metropolis-Hastings

```

Start:  $\vec{\theta}_1, \rho = 1, \Sigma = \mathbb{1}$ 
for  $i = 1, \dots, n$ 
  evaluate  $\mathbf{Q}$  by Cholesky decomposition of  $\Sigma$ 
  normalize  $\mathbf{Q} \rightarrow \mathbf{Q}/\det(\mathbf{Q})^{1/D}$ 
  propose move  $\vec{y} = \vec{\theta}_i + \rho \mathbf{Q} \cdot \vec{\eta}$  with  $\vec{\eta} \sim \mathcal{N}(\vec{0}, \mathbb{1})$ 
  evaluate ratio  $\mathcal{P}(\vec{y})/\mathcal{P}(\vec{\theta}_i)$ 
  if accepted
     $\vec{\theta}_{i+1} = \vec{y}$ 
     $\rho \rightarrow f_e \rho$ 
     $\Sigma \rightarrow \left(1 - \frac{1}{N_C}\right) \Sigma + \frac{1}{N_C} (\vec{\theta}_{i+1} - \vec{\theta}_i) (\vec{\theta}_{i+1} - \vec{\theta}_i)^T$ 
  if rejected
     $\vec{\theta}_{i+1} = \vec{\theta}_i$ 
     $\rho \rightarrow f_c \rho$ 
     $\Sigma \rightarrow \Sigma$ 

```

The structure of the adaptive Metropolis-Hastings algorithm used in the MCMC is the following: we start from an initial state $\vec{\theta}_1$, setting $\rho = 1$ and $\Sigma = \mathbf{Q} = \mathbb{1}$, where $\mathbb{1}$ is the identity matrix. Then, at each step a new point is sampled as

$$\vec{\theta}_{i+1} = \vec{\theta}_i + \rho \mathbf{Q} \cdot \vec{\eta}, \quad (11)$$

where $\vec{\eta}$ is drawn from a Gaussian distribution with zero mean and unit variance $\mathcal{N}(\vec{0}, \mathbb{1})$. If the proposed move $\vec{\theta}_{i+1}$ is accepted, the step size and the covariance matrix are updated according to the following rules:

$$\rho \rightarrow f_e \rho, \quad (12)$$

$$\Sigma \rightarrow \left(1 - \frac{1}{N_C}\right) \Sigma + \frac{1}{N_C} (\Delta \vec{\theta}) (\Delta \vec{\theta})^T, \quad (13)$$

where $f_e > 1$ is called *expansion factor*, N_C is a free parameter of the GaA and $\Delta \vec{\theta} = \vec{\theta}_{i+1} - \vec{\theta}_i$. Conversely, if the proposed jump is rejected, the covariance matrix is not updated and the step size is reduced by a *contraction*

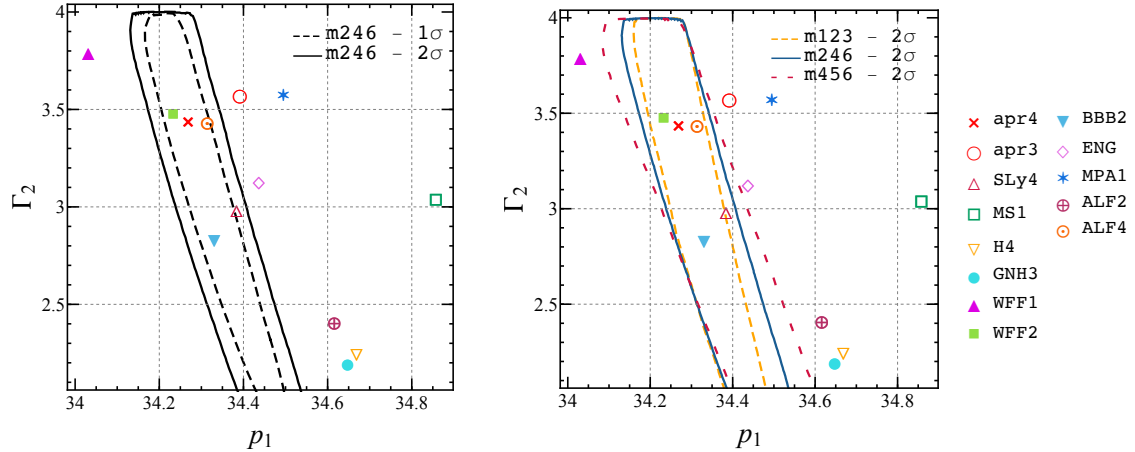


FIG. 7. (Left) 2-D credible regions at 1- and 2σ level for the joint probability distribution $\mathcal{P}(p_1, \Gamma_2)$, computed assuming **apr4** as the true equation of state (red cross), for the model **m246**. Different markers correspond to the values of p_1 and Γ_2 for various EoS. (Right) Comparison among the 2σ intervals of $\mathcal{P}(p_1, \Gamma_2)$ derived for the three models considered in this paper.

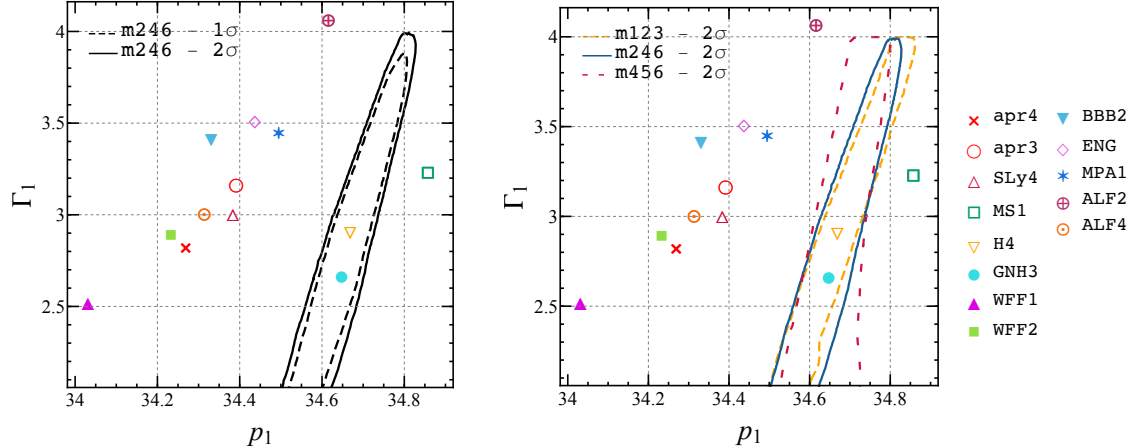


FIG. 8. (Left) 2-D credible regions at 1- and 2σ level for the joint probability distribution $\mathcal{P}(p_1, \Gamma_1)$, for **h4** as the true equation of state (yellow triangle), for the model **m246**. Different markers correspond to the values of p_1 and Γ_1 for various EoS. (Right) Comparison among the 2σ intervals of $\mathcal{P}(p_1, \Gamma_1)$ derived for the three models considered in this paper.

factor $f_c < 1$:

$$\rho \rightarrow f_c \rho \quad , \quad \Sigma \rightarrow \Sigma . \quad (14)$$

The GaA algorithm relies on some free parameters, which following [32], we have fixed to the following values:

$$\begin{aligned} f_e &= 1 + \beta(1 - P) \\ f_c &= 1 - \beta P \\ \beta &= 1/N_C \\ N_C &= (D + 1)^2 / \log(D + 1), \end{aligned} \quad (15)$$

where D is the dimension of the MCMC parameter space

and P is the acceptance probability of the proposed move. For our simulations we find an optimal value of such probability, which guarantees an efficient mixing of the chains, corresponding to $P = 0.25$. An example of the chain generated with this algorithm for the model **m246** and the EoS **apr4** is shown in Fig. 9.

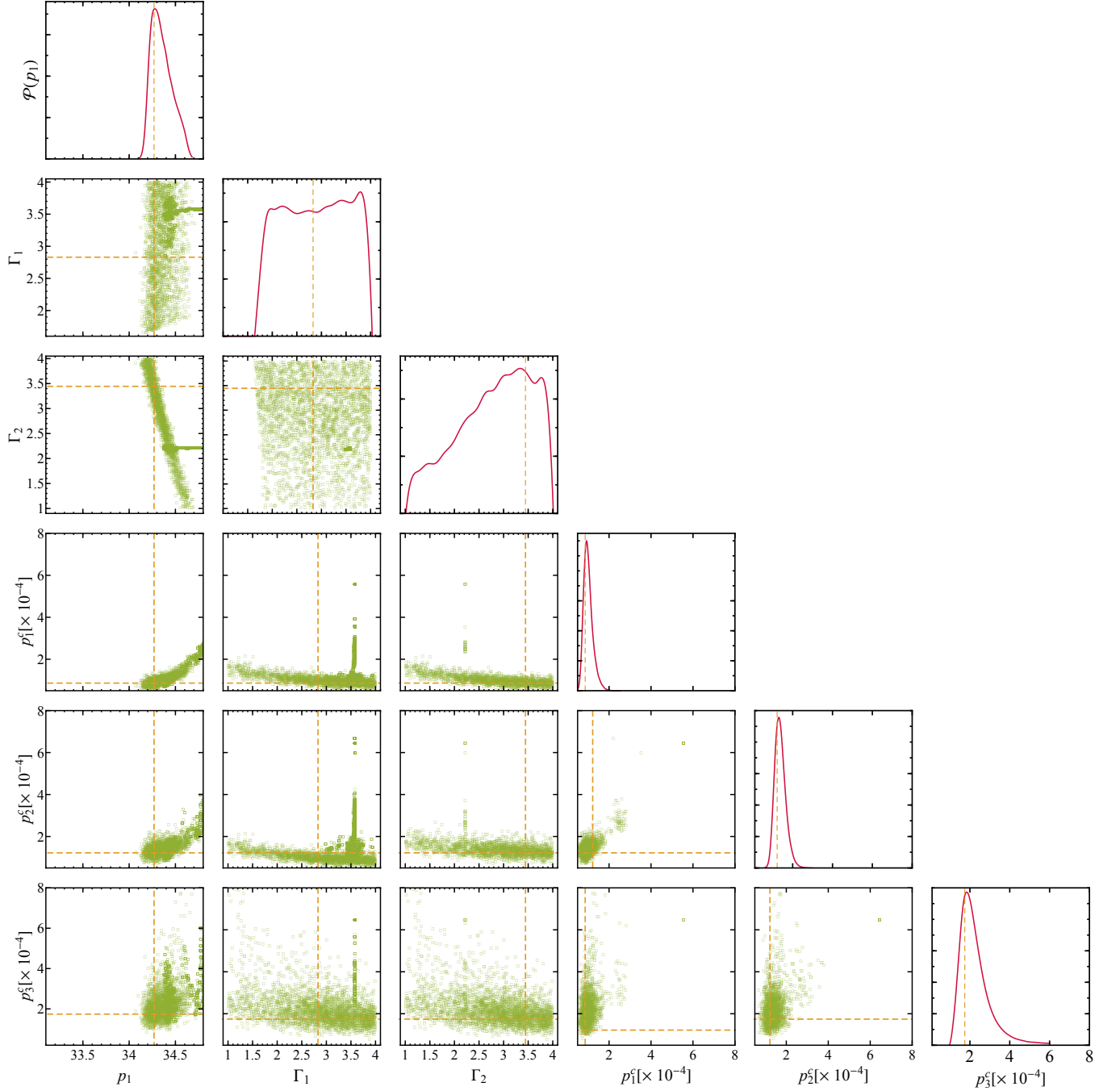


FIG. 9. An example of the chains produced by the GaA for the model `m246` and the EoS `apr4`. On the main diagonal we show the marginalized probability distribution of each parameter.

-
- [1] B. P. Abbott *et al.* (LIGO Scientific Collaboration and Virgo Collaboration), *Phys. Rev. Lett.* **116**, 061102 (2016).
- [2] B. P. Abbott *et al.* (LIGO Scientific Collaboration and Virgo Collaboration), *Phys. Rev. Lett.* **116**, 241103 (2016).
- [3] B. P. Abbott *et al.* (LIGO Scientific and Virgo Collaborations), *Phys. Rev. Lett.* **118**, 221101 (2017).
- [4] B. P. Abbott *et al.* (LIGO Scientific Collaboration and Virgo Collaboration), *Phys. Rev. Lett.* **119**, 141101 (2017).
- [5] B. P. Abbott *et al.* (LIGO Scientific Collaboration and Virgo Collaboration), *Phys. Rev. Lett.* **119**, 161101 (2017).

- [6] B. P. Abbott *et al.*, *Astrophys. J. Lett.* **848**, L12 (2017).
- [7] J. M. Lattimer and M. Prakash, *Astrophys. J.* **550**, 426 (2001).
- [8] L. Lindblom, *Astrophys. J.* **398**, 569 (1992).
- [9] T. Hinderer, B. D. Lackey, R. N. Lang, and J. S. Read, *Phys. Rev. D* **81**, 123016 (2010).
- [10] T. Damour, A. Nagar, and L. Villain, *Phys. Rev. D* **85**, 123007 (2012).
- [11] A. Maselli, L. Gualtieri, and V. Ferrari, *Phys. Rev. D* **88**, 104040 (2013).
- [12] B. D. Lackey, K. Kyutoku, M. Shibata, P. R. Brady, and J. L. Friedman, *Phys. Rev. D* **89**, 043009 (2014).
- [13] B. D. Lackey, K. Kyutoku, M. Shibata, P. R. Brady, and J. L. Friedman, *Phys. Rev. D* **85**, 044061 (2012).
- [14] B. D. Lackey and L. Wade, *Phys. Rev. D* **91**, 043002 (2015).
- [15] L. Wade, J. D. E. Creighton, E. Ochsner, B. D. Lackey, B. F. Farr, T. B. Littenberg, and V. Raymond, *Phys. Rev. D* **89**, 103012 (2014).
- [16] J. A. Clark, A. Bauswein, N. Stergioulas, and D. Shoemaker, *Classical Quantum Gravity* **33**, 085003 (2016).
- [17] S. Bose, K. Chakravarti, L. Rezzolla, B. S. Sathyaprakash, and K. Takami, *Phys. Rev. Lett.* **120**, 031102 (2018).
- [18] T. Hinderer, *Astrophys. J.* **677**, 1216 (2008), **697**, 964(E) (2009).
- [19] T. Damour and A. Nagar, *Phys. Rev. D* **80**, 084035 (2009).
- [20] T. Binnington and E. Poisson, *Phys. Rev. D* **80**, 084018 (2009).
- [21] F. Ozel and P. Freire, *Ann. Rev. Astron. Astrophys.* **54**, 401 (2016).
- [22] L. Lindblom and N. M. Indik, *Phys. Rev. D* **89**, 064003 (2014).
- [23] T. Abdelsalhin, A. Maselli, and V. Ferrari, (to be published).
- [24] L. Lindblom, *Phys. Rev. D* **82**, 103011 (2010).
- [25] L. Lindblom and N. M. Indik, *Phys. Rev. D* **86**, 084003 (2012).
- [26] J. S. Read, B. D. Lackey, B. J. Owen, and J. L. Friedman, *Phys. Rev. D* **79**, 124032 (2009).
- [27] A. W. Steiner, J. M. Lattimer, and E. F. Brown, *Astrophys. J.* **722**, 33 (2010).
- [28] C. A. Raithel, F. Özel, and D. Psaltis, *Astrophys. J.* **844**, 156 (2017).
- [29] C. A. Raithel, F. Özel, and D. Psaltis, *Astrophys. J.* **831**, 44 (2016).
- [30] F. Ozel and D. Psaltis, *Phys. Rev. D* **80**, 103003 (2009).
- [31] W. Gilks, S. Richardson, and D. Spiegelhalter, *Markov Chain Monte Carlo in Practice*, Chapman & Hall/CRC Interdisciplinary Statistics (Taylor & Francis, London, 1995).
- [32] C. L. Müller and I. F. Sbalzarini, in *IEEE Congress on Evolutionary Computation* (2010) pp. 1–8.
- [33] B. P. Abbott *et al.*, *Astrophys. J. Lett.* **848**, L13 (2017).
- [34] M. Vallisneri, *Phys. Rev. D* **77**, 042001 (2008).
- [35] <https://dcc.ligo.org/cgi-bin/DocDB>ShowDocument?docid=2974>.
- [36] <https://dcc.ligo.org/LIGO-P1200087-v19/public>.
- [37] <http://gwcenter.icrr.u-tokyo.ac.jp/en/researcher/parameter>.
- [38] C. L. Rodriguez, B. Farr, V. Raymond, W. M. Farr, T. B. Littenberg, D. Fazi, and V. Kalogera, *Astrophys. J.* **784**, 119 (2014).
- [39] W. Del Pozzo, T. G. F. Li, M. Agathos, C. Van Den Broeck, and S. Vitale, *Phys. Rev. Lett.* **111**, 071101 (2013).
- [40] G. Kjellstrom and L. Taxen, *IEEE Transactions on Circuits and Systems* **28**, 702 (1981).